Investigation of Thermal Regime Across the San Jacinto Fault

Tien-Chang Lee
University of California
Institute of Geophysics and Planetaty Physics

USGS CONTRACT NO. 14-08-0001-17714
Supported by the EARTHQUAKE HAZARDS REDUCTION PROGRAM

OPEN FILE NO. 80-1151

METHOD

Site Selection

A profile across the San Jacinto fault near Anza, southern California is chosen to investigate whether a local heat flow anomaly may associate with an active strike-slip fault. This specific profile is selected for the following reasons:

First, the San Jacinto fault is nearly half way between two other major strike-slip faults, Mission Creek and Elsinore faults, of the San Andreas fault system in southern California (Fig. 1). It is wished that, if indeed faulting can create a heat flow anomaly, the thermal contribution from the Mission Creek and Elsinore faults would have been nearly equal to each other and an anomaly would be symmetric with respect to the San Jacinto fault. To the north, in the Cajon Pass-San Bernardino-Riverside area, the bending of the San Andreas fault, and Banning-Mission Creek fault can complicate further the thermal regime. In other words, one would like to treat the fault-related thermal regime as a two dimensional problem for analysis before the relation can be clearly demonstrated.

Second, the tonalite of the southern California batholith as described in the Geological Maps (Santa Ana Sheet) by California Division of Mines and Geology and by Sharp (1967) appears on both sides of the San Jacinto fault. Lithological similarity can minimize the effect of refraction across media of different thermal conductivity and possibly the effect of different radioactive heat generation rate. Field inspection indicates, however, that the San Jacinto Mountain on the northeastern side of the fault trace is rugged and the rocks appear relatively fresh. On the southwestern side, the topography is subdued and the rocks appear fairly weathered to an unknown depth extent.

Third, three measurements made by Henyey and Wasserburg (1971) on the southwestern side of the San Jacinto fault trace show a possible anomaly of 0.3 μ cal/cm^{2}sec. It is imperative to extend their profile further away and, in particular, to the northeast side so as to verify the existence of an anomaly.

Once the profile had been selected, the sites were chosen on the compromise between the budgeted drilling cost and the regional-local separation of heat flow values. Attention was paid to avoid sites with large local relief and spring activity. Ideal sites are not readily available because of the environmental impact of drilling a 4-inch borehole on the wildlife, destruction of suspected archeological sites, residential development and permission to drill.

Six holes were drilled to ~100 m each. Coring was attempted in each borehole only for the bottom 10 m. Rock chips were collected at 3.3 m intervals (10 ft). The holes were cased with 2-inch PVC pipe. The annulus between the pipe and well bore was backfilled with the rock chips.

Sites E3 and E2 at distance of 16 and 7 km, respectively, from the fault trace were drilled into the tonalite on the San Jacinto Mountain (Fig. 1, Table 3). Rock chips indicate the rocks are fairly fresh at depth below ~10 m.

Sites W1 and W2 were also drilled in the tonalite as shown on the geological map but the rocks on the surface are fairly weathered. At site W1, the rocks appear weatehred throughout the 100 m borehole. However, core recovery was good. The hole collapsed before the PVC pipe was installed. Rocks at site W2 appear to have been weathered only to a depth of 30 m. The recovered core contains a streak of fresh pyrite.

The intent of drilling at E1 on the northeastern side of the San Jacinto fault was to provide a counterpart to sites AN1 and AN3 of Henyey and Wasserburg (1971) on the southwestern side of the fault. The Mid-Cretaceous tonalite

in the vicinity but to the northeast of the fault is inaccessible to the drill truck. The Pre-Mid-Cretaceous metamorphic rocks near the fault is also inaccessible. Site E1 was drilled only because it was not possible to find an ideal site. Rock chips and cores indicate the borehole has penetrated only the sedimentary rocks which were derived from the nearby plutonic and metamorphic rocks.

Site N1 is located about 25 to 30 km from the Anza profile. It provides a measurement of how far the anomaly may persist to the north if the anomaly exists. The site could have been located on the northeastern side of the fault as a supplement to site E1 if the tonalite on the northeastern side were accessible. Local relief also precludes an ideal site to be located there on the northeastern side of the San Jacinto fault.

Temperature Measurement

Temperature in the borehole was measured with a thermistor probe. The thermistor has a nominal resistance of 10,000 ohms at 25°C. The time constant of the probe-cable assemblage is ∿10 S. A Wheatstone bridge is used to measure the equilibrium resistance of the thermistor.

The equilibrium temperature is converted from the measured resistance through a calibration curve of the type,

$$1/T = \alpha + \beta \ln R + \gamma (\ln R)^3 \qquad (1)$$

where T = absolute temperature, R = resistance. The calibration constants α, β, and γ are determined for the probe and cable assemblage in the temperature range from 0 to 50°C at 5°C intervals with reference to a quartz thermometer (HP 280). The maximum difference between the observed and fitted temperature is 0.004°C. The resolution is ∿0.001°C and the accuracy is believed to be ∿0.01°C.

Lead wire resistance and shant resistance are automatically compensated through the use of a 4-conductor cable. The current through the thermistor at equilibrium is less than 10 μA (or equivalently, ~50 μW) so self-heating effect is negligible.

The depth of temperature measurement is determined with pre-determined marking on the logging cable. Stretching in the cable is considered negligible for our maximum logging depth of 100 m. The temperatures in the borehole were read at 5 m intervals.

Conductivity Measurements

A divided-bar apparatus is used to measure thermal conductivity of rocks. The copper bars and samples are enclosed tightly by cylinders made of styrofoam, of which the diameter is at least 2.5 times greater than the sample diameter. The upper bar is maintained by circulating water at 30°C and the lower bar at 20°C. Therefore, sample temperature is maintained at 25°C and radial heat loss through the cylindrical surface of the styrofoam insulator can be further reduced. A hydraulic pressure of 100 bars is applied axially to the bar-sample-bar assemblage to reduce the contact thermal resistance. Each sample was coated with thin film of silicon grease before its being inserted in the apparatus for measurement.

The apparatus is calibarated with a circular cylinder made of fused silica (diameter D = 5.5 cm, height H = 3.81 cm). Temperature is measured at two positions in the upper bar (T_1 and T_2) and lower bar (T_3 and T_4). A calibration constant C is then obtained from

$$C = \frac{T_2 - T_3}{(T_1 - T_2) + (T_3 - T_4)} \frac{K}{H} \qquad (2)$$

where K is the known conductivity of fused silica.

If the radial heat loss for the standard and sample is identical, the conductivity of a sample k_1 is then given by

$$k_1 = \frac{(T_1 - T_2) + (T_3 - T_4)}{T_2 - T_3} Ch \qquad (3)$$

where h is the thickness of the sample. The sample disk has been cut to make its thickness be as close to the thickness of fused-silica standard as possible. The diameter of sample d is slightly less than that of the standard. Hence, k_1 in Eq. (3) is regarded as the apparent conductivity. The true conductivity k of the sample is corrected, using steady-state heat conduction theory, from the apparent conductivity by

$$k = (k_1 - k_s) \frac{D^2}{d^2} + k_s \qquad (4)$$

To see the limit in using Eq. (3) and Eq. (4), the conductivity for disks of fused silica and crystalline quartz (cut parallel to the c-axis) of the same height H but smaller diameter was determined. Repeated measurements through mounting and dismounting the styrofoam insulator indicate the errors of individual measurements for fused silica are $\pm$ 2% while for crystaline quartz the error may run up to $\pm$ 7%. Because the conductivities of rocks lie between those of fused silica and crystalline quartz, the errors for rocks can be linearly interpolated. However, the diameter of rock sample is greater than that of the tested standards, therefore, the actual error should be less than that given by linear interpolation. The values reported by Ratcliffe (1959) for fused silica and crystalline quartz is used throughout the calibration of the apparatus.

Because coring was limited to reduce the cost of drilling, attempt has been made to determine the thermal conductivity from the rock chips. The chips are placed in a plastic container which has the same height as the

reference standard of fused silica but its diameter is smaller. The void in the container is filled with water and covered with a plastic lid. The measurement procedures are the same as for the rock disks. The data reduction procedures follow those described by Sass et al. (1971) with modification.

From Eqs. (3) and (4), the conductivity k_2 for the plastic container and the water-rock mixture is determined. The contribution of the top and bottom lids is then stripped, using the relation

$$\frac{H}{k_2} = \frac{2t}{k_p} + \frac{H-2t}{k_3} \tag{5}$$

where t = thickness of lid and k_p = conductivity of plastic, and k_3 = the conductivity of plastic wall and rock-water mixture.

The contribtution of plastic wall is removed, using an equation similar to Eq. (4).

$$k_4 = (k_3 - k_p) \frac{d^2}{(d-W)^2} + k_p \tag{6}$$

where w = wall thickness and k_4 is the conductivity of rock-water mixture.

The conductivity is finally obtained from

$$k_4 = k^{1-\phi}\, k_w^{\phi} \tag{7}$$

where k_w = conductivity of water and ϕ is the porosity of the rock-water mixture. The porosity is calculated as the ratio of water volume, converted from the mass of water added to the plastic container assuming a density of 1 g/cm^3, to the inner volume of the container.

The conductivity of plastic used in Eqs. (5) and (6) is determined from a stack of plastic sheet, using Eq. (3). The conductivity of styrofoam used in equation (3) is determined from the needle probe method. Care was taken to

avoid melting of styrofoam around the needle heat source. The values for plastic and styrofoam are on the same order of magnitude reported for plastic and styrofoam in general.

RESULT

Thermal Conductivity

The results of thermal conductivity measurements are presented in Tables 1 and 2 for core samples and chip samples, respectively. Coring was limited to the bottom 10 m in each borehole. Some cores are too distorted for making cylindrical disks. Fractures in some cases also prevent disks from being made. For example, there are only two acceptable disks made from 10 m cores at site W2. The number of samples shown on Table 1 for each site reflect grossly the condition of cores.

There appears to be no systematic variation in thermal conductivity for the cores sampled. A few relatively low values appear to correlate visually with cracks in the disks. For this reason, one value for site E2 and three values for site E3 are excluded from the calculation of the mean value for each hole. The standard deviations for individual boreholes range from 4 to 8% of their respective means.

The chip samples were measured at ~3.3 m (10 ft) invervals. At site E3 the conductivity tends to increase slightly with depth whereas at other sites there appears to have been no systematic variation at depths below 33 m (100 ft). Erratic values appear occasionally in the measurements of chip samples. Samples with values above 7 or below 5×10^{-3} cal/cm°C sec were measured twice. If the two did not agree within 5% of their mean, the values were discarded. Random checks were also made for samples with conductivity values lying between 5 and 7×10^{-3} cal/cm°C sec.

The conductivity values measured from chip samples and core samples agree, in general, well with one another. For sites E2 and W2, the mean value of chip samples differs from the average of the means for chip and core samples

by less than 2.4%. For site E3, the difference is 6%. However, for site W1, the difference is 16.8%. This large difference is attributable to poor sample preparation for cores. The tonalite at site W1 is fairly weathered and the edge of the sample disk was always worn out during sawing and polishing. The low values reported for the core samples were the consequence of high contact thermal resistance between the copper bar and core disk. Hence, the mean conductivity for chip samples is used in the estimate of heat flow.

For site E1, the cores were not suitable for making disk. The mean conductivity for chip samples is therefore used. At site N1, the chip samples were not measured and the comparison with core samples cannot be made.

Geothermal Gradient

Temperature versus depth profiles are presented in Figures 2, 3, 4, 5, 6 and 7 for sites W2, W1, N1, E1, E2, and E3, respectively, ordered from the southwest to northeast across the San Jacinto fault. Four measurements were made in each of six wells form June, 1979 to March, 1980. The measured gradients vary less than 4% at individual sites for the depth range of 50 to 100 m. Because the measurements were made both in the wet and dry seasons, the effect of seasonal groundwater fluctuation on the geothermal gradients appears to be negligible in those sites. The effect of deeper circulation and secular variation in the water table, however, cannot be assessed for the present depth and duration of observation.

Geothermal gradients shown on Table 3 are the slopes of a straight line fitted by the least-squares method to the temperature-depth profiles from 50 to 100 m at 5 m intervals. A steady-state three dimensional topographic correction (Birch, 1950) assuming a lapse rate of 4.5°C/km, has been applied. This topographic correction amounts to about 1~2%. The means for four

temperature-depth profiles measured at different times are used for the calculation of heat flow at individual sites.

The gradients are 11, 15, 27, 27, 19 and 17 C°/km at the distance of -20, -5, -1, 0.5, 7, and 16 km from the fault trace, respectively (negative and positive signs are for sites to the southwest and northeast of the fault, respectively). For comparison, the gradients reported earlier by Henyey and Wasserburg (1971) are 23, 25 and 24°C/km at the distance of -13, -4, -1 km, respectively. The gradient 15°C/km at -5 km is significantly less than the gradient 25°C/km at -4 km. Because the gradient at site W1 (-5 km) was obtained for the depth range from 35 to 50 m, the quality of the data is not as good as those at other sites. The gradient at site W1 is hence inferior to the value at site AN-1 of Henyey and Wasserburg and it cannot be used for quantitative study.

Heat Flow

The products of geothermal gradients and conductivities gives the heat flux at individual sites (Table 3). Conductivity values measured from the core samples are used in the calculation of heat flow except at W1 where the core disk samples show high contact thermal resistance and at E1 where the cores are not suitable for making disk samples.

Six heat-flow values obtained in this study and three values by Henyey and Wasserburg show the heat flow in the study area of the southern California batholith is low to normal, from 0.65 to 1.87 $\mu cal/cm^2 sec$ or 27 to 78×10^{-3} W/m^2. Those values are typical of the heat flows in the Peninsular Ranges. The distribution shows clearly the heat flow increase toward the San Jacinto fault (Fig. 8). The values are 0.65, 1.46, 0.84, 1.87, 1.72, 1.76 $\mu cal/cm^2 sec$ at the distances of -20, -13, -5, -4, -1 and -1 km, respectively on the southwestern side of the fault while they are 1.40, 1.18 and 0.94 at the distance of 0.5, 7, 16 km on the northeastern side, respectively.

It is noted that heat flows were determined for depth below 110 m by Henyey and Wasserburg (1971), but in this study the depth range is from 50 to 100 m. Their geothermal gradients for 10-m intervals appear to increase slightly with depth for depth less than 100 m. Because the conductivity data were not readily available, it is not clear whether there is a systematic variation in the 10-m interval heat flows.

It is further noted that the heat generation rate was not measured. The difference in heat generation can contribute to variation in heat flow.

DISCUSSION

The results of this study indicate heat flows increase toward the San Jacinto fault. In the following, the magnitude of heat flow anomaly over the fault will be defined, then its implication on fault movement discussed.

Heat Flow Anomaly

In the work by Henyey and Wasserburg (1971), a possible anomaly of 0.3 $\mu cal/cm^2sec$ was defined for a 13-km profile to the southwest of the San Jacinto fault near Anza. It was questioned then for lack of data that the anomaly might reflect in part the regional transition from the low heat-flow Peninusula Ranges to the high heat-flow Imperial Valley. New values at sites E1 and E2 indicate heat flow decreases northeastward to the Imperial Valley. Therefore, the existence of an anomaly over the San Jacinto fault can now be ascertained.

As noted earlier, the quality of data in the shortened borehole at site W1 precludes the heat-flow value there from quantitative estimation of the anomaly. Because site E1 is located in the sediments derived from pre-Mid-Cretaceous metamorphic rocks on the northeastern side of the San Jacinto fault. Across the fault, the area is presumably tonalite but covered by alluvium with unknown thickness. It is not clear how much heat-flux refraction across the dissimilar media can contribute to the relatively low value at E1 (1.40 compared to 1.76 $\mu cal/cm^2sec$ at AN3). Furthermore, the radioactive heat production in the metamorphic rocks may differ from that in the plutonic rocks. The unknown difference enhances the uncertainty in the evaluation of the anomaly. Site E1 is so close to the fault trace that it may be more susceptible to the effect of long-term deeper water circulation in the fault zone even though repeated measurements suggest seasonal effect is negligible. For these reasons,

the value at site E1 is also tentatively excluded from further quantitative consideration.

Excluding values at W1 and E1, the heat-flow distribution as shown in Fig. 8 appears to be asymmetric about the fault trace. Because the San Jacinto fault lies almost half-way between the Mission Creek fault and the Elsinore fault, the heat-flow distribution is expected to peak over the San Jacinto fault and decrease away from it if frictional heat dissipation is symmetric about a single fault and the contributions from the Mission Creek and Elsinore faults are equal to each other. However, regional heat-flow variation can distort the expected symmetric distribution.

The mean for three values nearest to the fault trace (AN1, AN3, and N1) is taken as the peak value over the fault. So the heat flow decrease from a peak value of 1.78 to 0.94 $\mu cal/cm^2sec$ over a distance of 16 km on the northeastern side of the fault and to 0.65 $\mu cal/cm^2sec$ over a distance 20 km on the southwestern side. From the available data along this 36-km profile, a background value cannot yet be determined undisputedly.

In the area close to the Elsinore fault, many unnamed faults have been reported on the geological map (Santa Ana Sheet, California Division of Mines and Geology). Large-scale groundwater circulation may have reduced the regional value. Microfractures or cracks shown on the cores recovered at site W2 makes one wonder about the effect of water circulation on the measured value there. Scattered water wells in the area suggest further that the effect cannot be simply disregarded if the value at site W2 is to be used quantitatively. For lack of sufficient information to evaluate the quality of the heat flow value at W2, the middle point between AN2 and W2 on Fig. 8 will be used somewhat arbitrarily to define the anomaly pattern as outlined by the dashed curve.

The heat flow distribution as outlined by the dashed curve seems to be somewhat symmetric about the fault trace. The background value is ∿1.0 μcal/cm^{2}sec. The anomaly has a peak value of 0.8 (=1.78-1.0) μcal/cm^{2}sec and a halfwidth of ∿7 km. Because site N1 is ∿30 km from the Anza profile and has essentially the same peak value, it may be stated that the anomaly persists along the fault for at least 30 km.

The area between the dashed curve and background value as shown on Fig. 8, represents the heat flow anomaly per unit fault length. Its value is approximately 1 cal/sec per cm of fault length. Assuming the anomaly has a width of 40 km, the mean of the anomaly is 0.25 μcal/cm^{2}sec, which is about one third of the heat-flow anomaly associated with the San Andreas fault zone, 0.8 μcal/cm^{2}sec, assumed by Lachenbruch and Sass (1973) for the California Coast Ranges over a width of ∿100 km.

Implications of the Anomaly

Various conceptual models can be built to explain the heat flow anomaly which is essentially described by a peak of 0.8 μcal/cm^{2}sec, halfwidth of 7 km, and mean anomaly of 0.25 μcal/cm^{2}sec over a zone 40 km wide along the fault trace. For simple strip-source models (Henyey and Wasserburg, 1971), one can vary the width, depth, and distribution of frictional heating to meet the characteristics of the anomaly. For more sophisticated models such as a brittle seismogenic layer over a ductile half space (Lachenbruch and Sass, 1973), one can also vary certain parameters to fit the observation. Nonuniqueness in the inversion of the data needs no illustration of various models to interpret an anomaly which is not yet unambiquously defined.

Faulting mechanism proposed by earthquake study and tectonic consideration should meet the energy constraint imposed by the anomaly. The question of how

much the observed short-term earthquake activity may represent the long-term tectonic process which create the anomaly adds the time dependency factor to the already complex study of faulting mechanism.

Before an acceptable explanation is given, a crucial question to ask is what is the unique nature of the San Jacinto fault which possesses a local heat-flow anomaly. An anomaly similar to the characteristics described earlier, if it exists, should have been recognized over other major strike slip faults. The San Andreas fault zone is relatively narrower in the California Coast Ranges and wider in the southern California region, particularly near the latitude of the study area. The heat generation rate is 8 cal/sec per centimeter of the length of the San Andreas fault zone in the Coast Ranges (=0.8 $\mu cal/cm^2 sec$ x 100 km). For the San Jacinto fault zone, which is one of the three major faults of the San Andreas fault zone in southern California, the heat generation rate is 1 cal/sec cm.

In terms of the frequency of moderate earthquakes ($6<M<7$), the San Jacinto fault zone is probably the most active one in the southern California region (Allen, 1975). It accounts for only 1/8 of the total heat output, assuming that the generation rate of 8 cal/sec cm holds throughout the San Andreas fault system. So, the observed anomaly results from concentration of heat generation near the San Jacinto fault. It is not necessary to invoke a model to have higher heat generation. The absence of a peaked anomaly elsewhere is due to the lack of resolution of the local value from the regional high heat flow.

Geologic correlation across the San Jacinto fault indicates the rate of displacement averages about 0.26 cm/yr since Pliocene time (Sharp, 1968), in contrast with 2.44 cm/yr estimated from geodetic survey across the San Jacinto fault zone near the Borrego Valley (Whitten, 1956). The displacement rate estimated from the total seismic moment for events with magnitude greater than

three during 1912-1963 averages 1.5 cm/yr (Brune, 1968). For nine events with magnitude greater than 6, Thatcher et al. (1975) obtained a value of 0.80 cm/yr for the interval 1890-1973 (or 0.46 cm/yr if the fault dimension and rigidity assumed by Brune are used). If all data are acceptable, the present rate of displacement appears to be higher than the average rate in the last 2 m.y. The time-dependent rate of displacement poses a problem in the modelling mentioned earlier.

On a smaller scale, the San Jacinto fault zone has also experienced different levels of seismic activity at different segments. The segment between a point ~10 km to the northwest of Anza and a point ~30 km to the southeast of Anza (Fig. 9) has been identified as one of two significant gaps in seismic slip along the San Jacinto fault zone (Thatcher et al., 1975). The other gap lies between the Cajon Pass and Riverside. These gaps are characterized at present by complex fault zones, high activity of minor earthquakes, and absence of aseismic creep. They may mark the sites of next moderate earthquakes (Thatcher et al., 1975). However, the segment between Riverside and Anza has experienced four moderate earthquakes during 1890-1923 with a total displacement of ~130 cm and shows a very low level activity of minor earthquakes as compared to the seismicity for the rest of the San Jacinto fault zone (Fig. 9). Hence the nature of faulting or displacement along the two segments to the northwest and southeast of Anza is quite different. The Anza heat-flow profile lies near the boundary of those two segments and the anomaly extends northward, for more than 30 km in the segment showing earthquake related displacement. It is not clear, however, whether the anomaly appears over both of the two segments.

CONCLUSION

Nine measurements indicate heat flows increase toward the San Jacinto fault. The shape of the anomaly and the background value cannot yet be undisputedly defined. Hence the values cited in this report must be regarded as tentative estimates to describe the configuration of the anomaly.

Heat generation rate per unit length along the San Jacinto fault is ~1/8 of that along the San Andreas fault in the Coast Ranges. The existence of a local heat-flow anomaly is attributed to favorable conditions for concentrating heat sources rather than higher heat generation rate along the San Jacinto fault.

TABLE 1 Thermal Conductivity Measurements of Core Samples

E2		E3		W1		W2		N1	
depth	K	depth	K	depth	K	depth	K	depth	K
308	6.55	310	5.54	315B	3.79	310	5.93	310.5	6.78
330	5.38*	311	4.66*	316.5	4.54	312	5.92	312	6.70
331.5	6.04	312	5.00*	319A	3.67			313	5.90
332.5	6.20	314	5.80	319B	4.01			313.5	6.79
336	6.40	315	5.61	319C	4.46			315	7.31
338	6.56	316	5.27	319D	4.02			316	5.87
		316.5	5.72	319E	4.04			316.5	6.26
		317	5.30	324	3.79				
		317.5	5.55	325A	3.78				
		320	5.94	325B	4.07				
		322	5.70						
		323	6.32						
		326	5.69						
		328	5.50						
		329	4.94*						
		330	5.41						
		330	6.09						
		331	5.61						
mean	6.19 ±0.25		5.54 ±0.29		4.02 ±0.29		5.92 ±0.01		6.39 ±0.54

Depth in feet
K = conductivity in units of 10^{-3} cal/cm°C sec
* = values not used in the calculation of the mean

TABLE 2 Thermal Conductivity Measurements of Rock Chips

E2		E3		W1		W2	
Depth	K	Depth	K	Depth	K	Depth	K
110	5.36	110	5.84	110	5.40	110	6.12
120	6.74	120	6.94	120	5.11	120	6.54
130	6.95	130	6.65	130	5.40	130	6.73
140	6.34	140	6.38	140	5.73	140	6.63
150	6.12	150	5.82	150	6.33	150	5.82
170	5.68	160	5.77	160	5.60	160	5.75
180	6.40	170	5.65	170	5.69	170	5.78
190	5.28	180	6.47	180	5.45	180	6.31
230	5.37	190	6.59	190	5.96	190	5.98
240	5.96	200	6.35			200	5.99
250	6.88	210	6.77			210	5.68
270	6.54	220	6.00			220	5.84
280	5.27	250				230	5.19
300	5.55	260	6.61			240	5.80
		290	6.90			250	6.73
		300				260	5.56
		310	6.33			270	5.75
						280	5.68
						290	5.70
						300	5.40
						310	5.73
						320	6.19
						340	6.20
mean	6.03		6.33		5.63		5.96

Depth in feet

K = conductivity in units of 10^{-3}cal/cm°C sec.

TABLE 3 Heat Fluxes Across the San Jacinto Fault

Site	E3	E2	E1	N1	W1	W2
Latitude 33°N	37' 00"	32' 30"	34' 06"	42' 15"	33' 36"	28' 40"
Longitude 116°W	25' 30"	30' 12"	37' 45"	53' 22"	42' 55"	50' 43"
Distance* km	+16	+7	+0.5	-1	-5	-20
Conductivity**	5.54 (18)	6.19 (6)	5.19 (8)+	6.39 (7)	5.63+(10)	5.92 (2)
Gradient °C/km	17	19	27	27	15	11
Heat Flux 10^{-} W/m	39	49	59	72	35	27
10^{-} cal/cm sec	0.94	1.18	1.40	1.72	0.84	0.65

*Distance to fault trace "+" for sites to the northeast of the fault and "-" for sites to the southwest of fault.

**Numbers in parentheses indicate number of samples measured.

+ Estimate from chip samples.

FIGURE CAPTIONS

Fig. No.

1 Generalized geological map along the San Jacinto fault zone (see Fig. 9 for its location). Solid circles denote new heat flow values and triangles denote data from Henyey and Wasserburg (1971).

2 Temperature profiles measured at different times at site W2.

3 Temperature profiles measured at different times at site W1.

4 Temperature profiles measured at different times at site N1.

5 Temperature profiles measured at different times at site E1.

6 Temperature profiles measured at different times at site E2.

7 Temperature profiles measured at different times at site E3.

8 Heat flow profile across the San Jacinto fault. Distance to the northeast of fault trace is positive; to the southwest it is negative. Dashed curve is the best estimate of the anomaly. Open circle is the middle point between AN2 and W2. Solid circles from this study, triangles from Henyey and Wasserburg.

9 Epicentral distribution (from Thatcher et al., 1975). (Left): All epicenters within the rectangular region are included. (Right): Epicenters not associated with the San Jacinto fault zone and after shocks are excluded. Abbreviations: C.P. = Cajon Pass; RVR = Riverside; S.J. = San Jacinto; A = Anza; C.M. = Coyote Mountain, S.M. = Superstition Mountain.

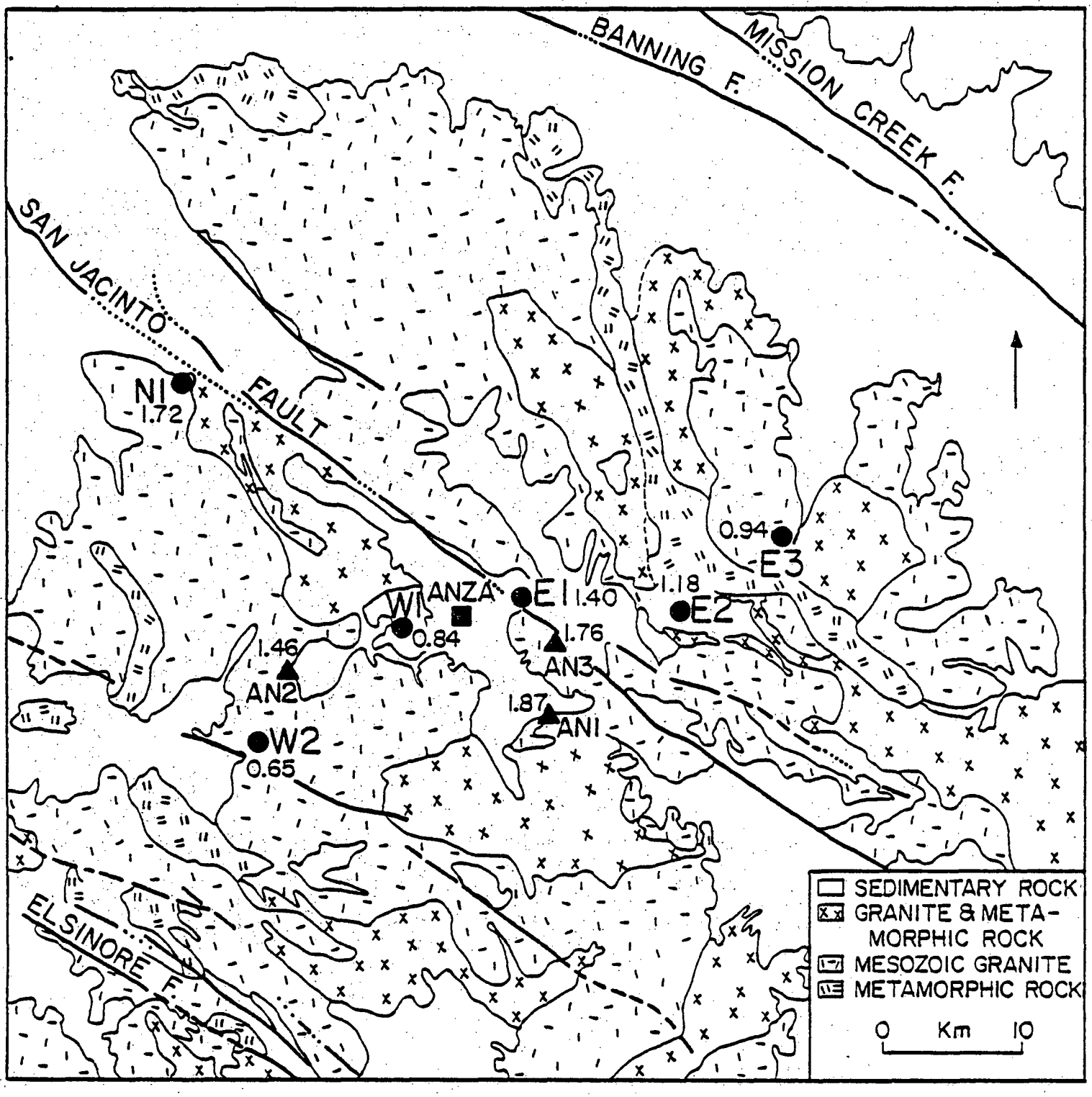
BANNING F.
MISSION CREEK F.
SAN JACINTO
FAULT
N1
1.72
0.94
E3
1.18
E2
W1
ANZA
E1
1.40
0.84
1.76
AN3
1.46
AN2
1.87
AN1
W2
0.65
ELSINORE F.
SEDIMENTARY ROCK
GRANITE & METAMORPHIC ROCK
MESOZOIC GRANITE
METAMORPHIC ROCK
0 Km 10

Figure 1

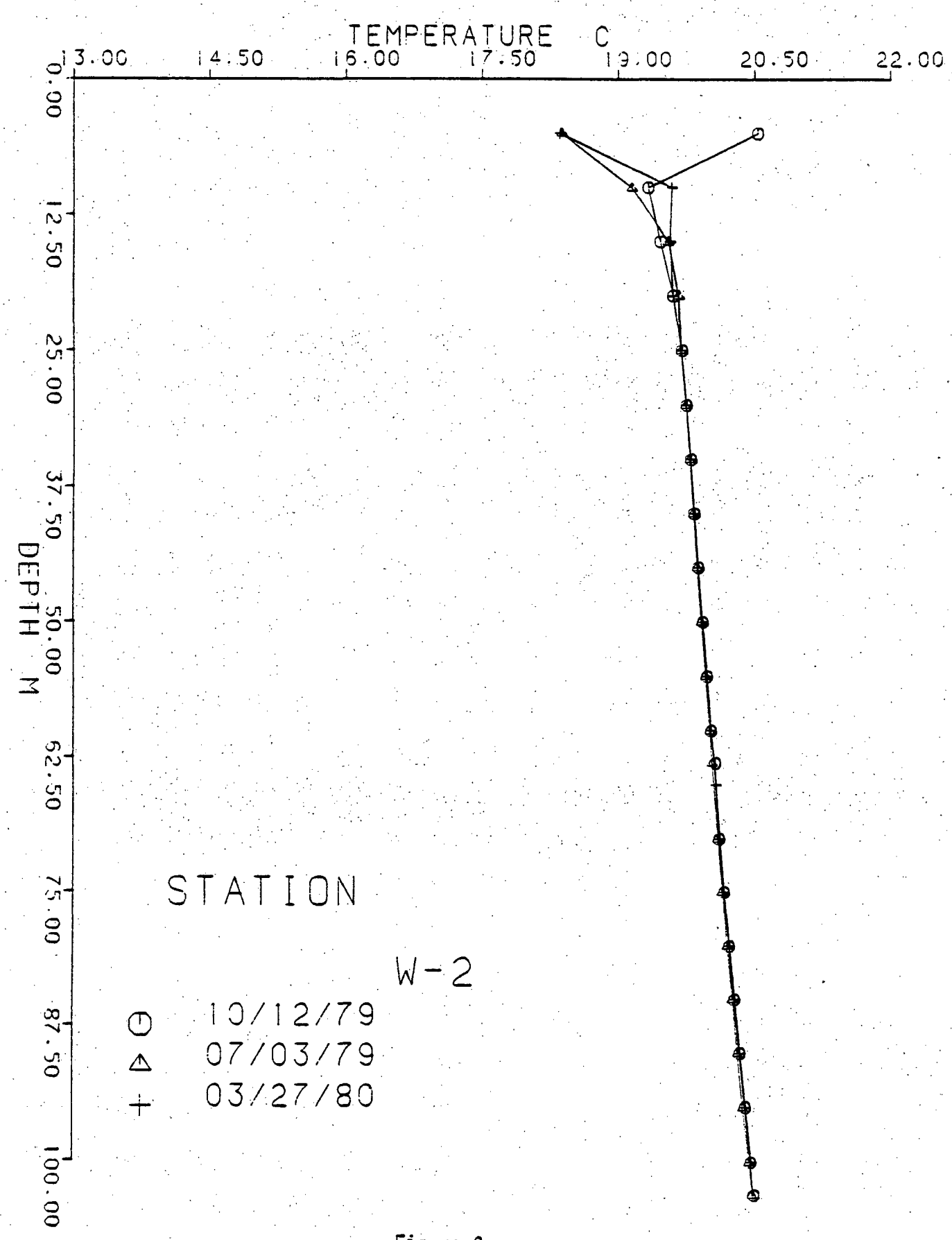
TEMPERATURE C
13.00
14.50
16.00
17.50
19.00
20.50
22.00
0.00
12.50
25.00
37.50
50.00
62.50
75.00
87.50
100.00
DEPTH M
STATION
W-2
10/12/79
07/03/79
03/27/80

Figure 2

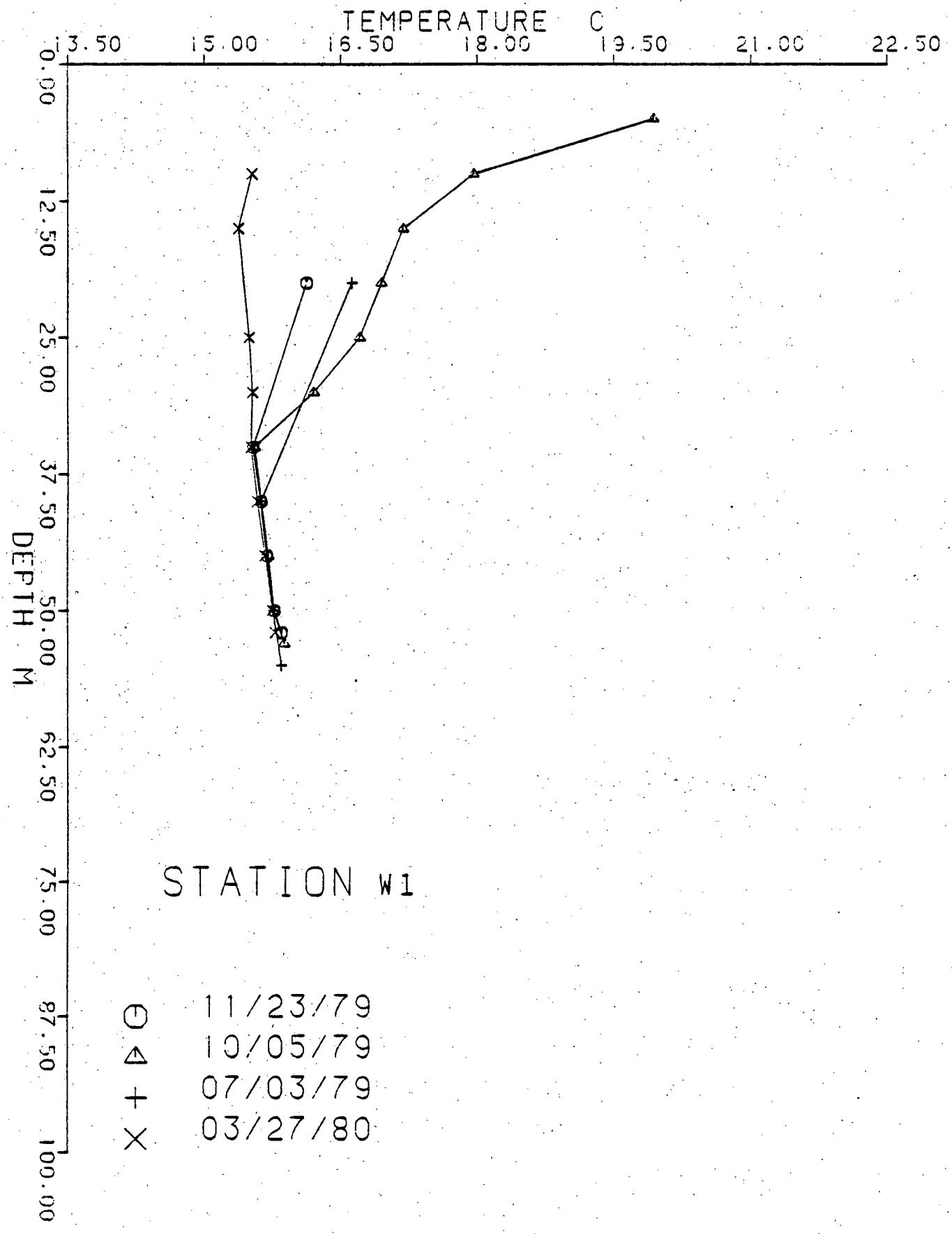
TEMPERATURE C
13.50
15.00
16.50
18.00
19.50
21.00
22.50
0.00
12.50
25.00
37.50
50.00
62.50
75.00
87.50
100.00
DEPTH M
STATION W1
Θ 11/23/79
Δ 10/05/79
+ 07/03/79
X 03/27/80

Figure 3

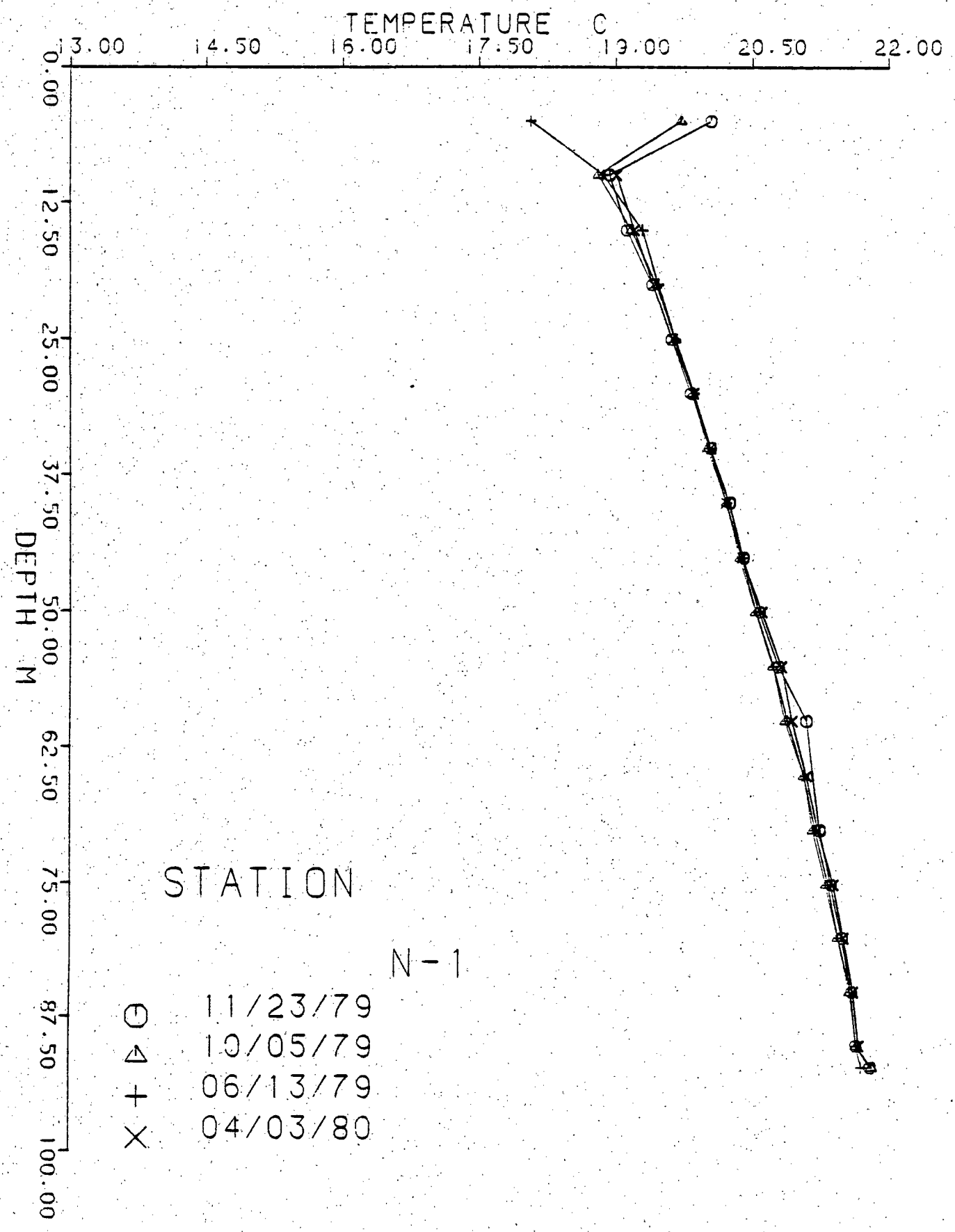
TEMPERATURE C
13.00
14.50
16.00
17.50
19.00
20.50
22.00
0.00
12.50
25.00
37.50
50.00
62.50
75.00
87.50
100.00
DEPTH M
STATION
N-1
11/23/79
10/05/79
06/13/79
04/03/80

Figure 4

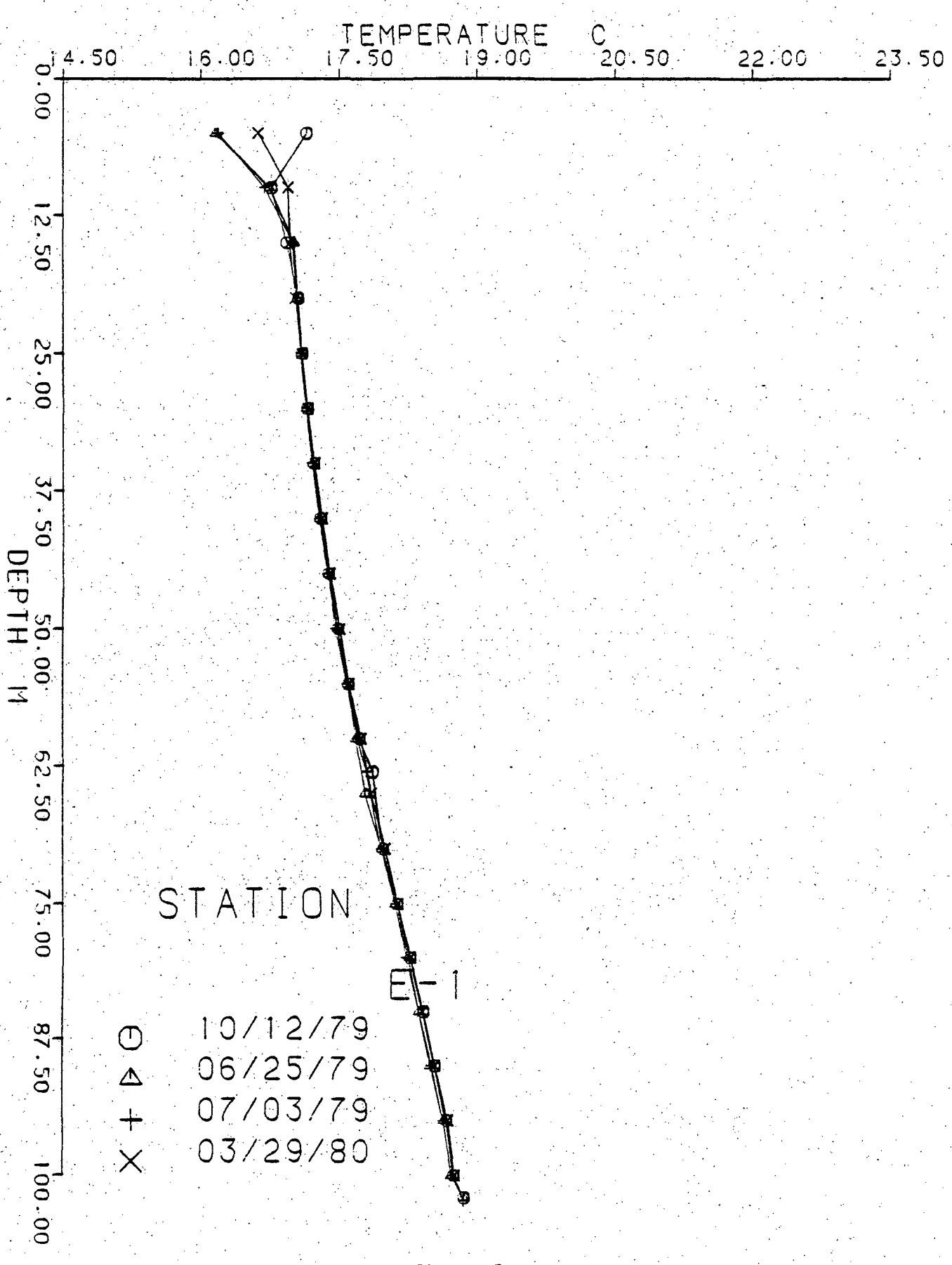
TEMPERATURE C
14.50
16.00
17.50
19.00
20.50
22.00
23.50
0.00
12.50
25.00
37.50
50.00
62.50
75.00
87.50
100.00
DEPTH M
STATION
E-1
10/12/79
06/25/79
07/03/79
03/29/80

Figure 5

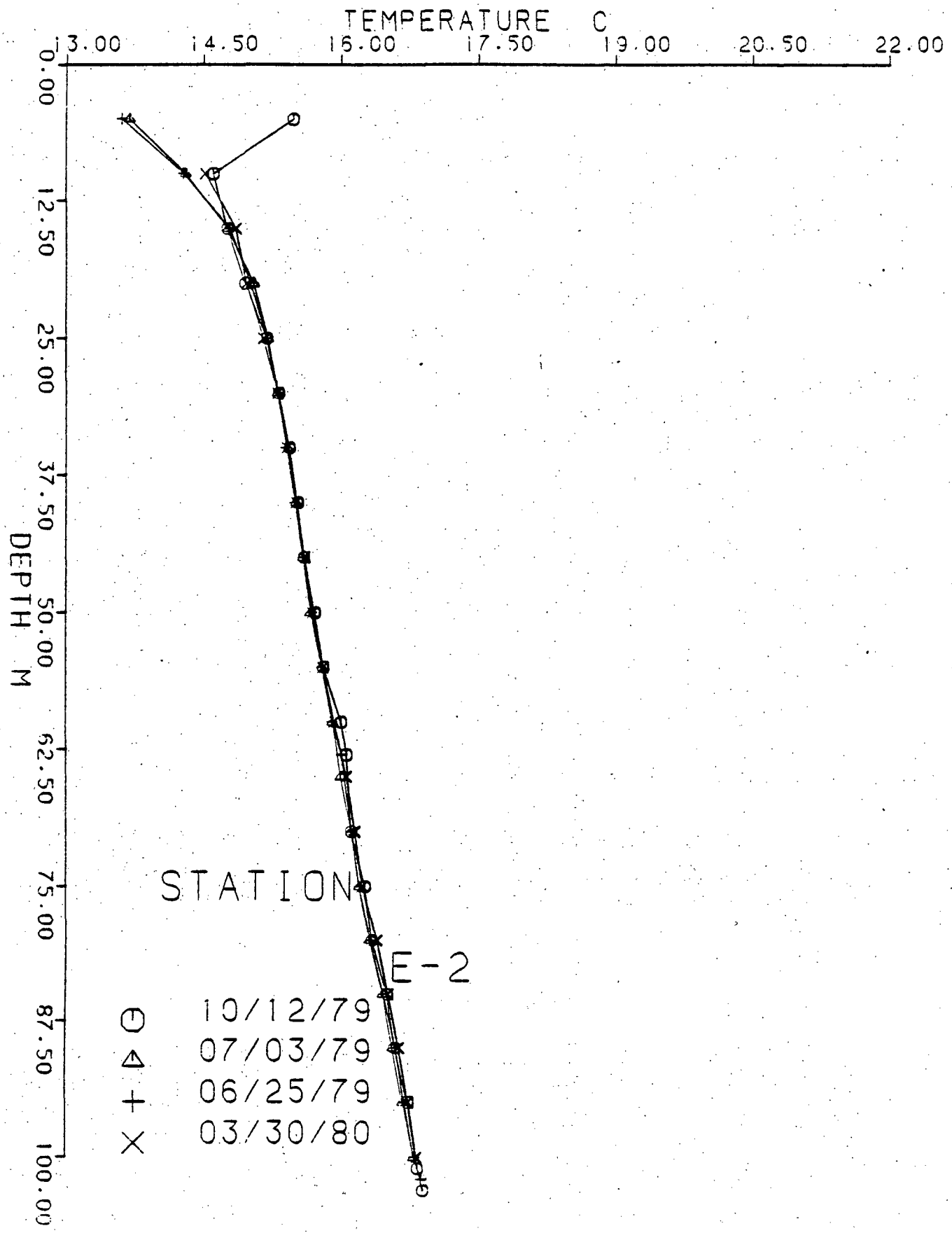
TEMPERATURE C
13.00
14.50
16.00
17.50
19.00
20.50
22.00
0.00
12.50
25.00
37.50
50.00
62.50
75.00
87.50
100.00
DEPTH M
STATION
E-2
10/12/79
07/03/79
06/25/79
03/30/80

Figure 6

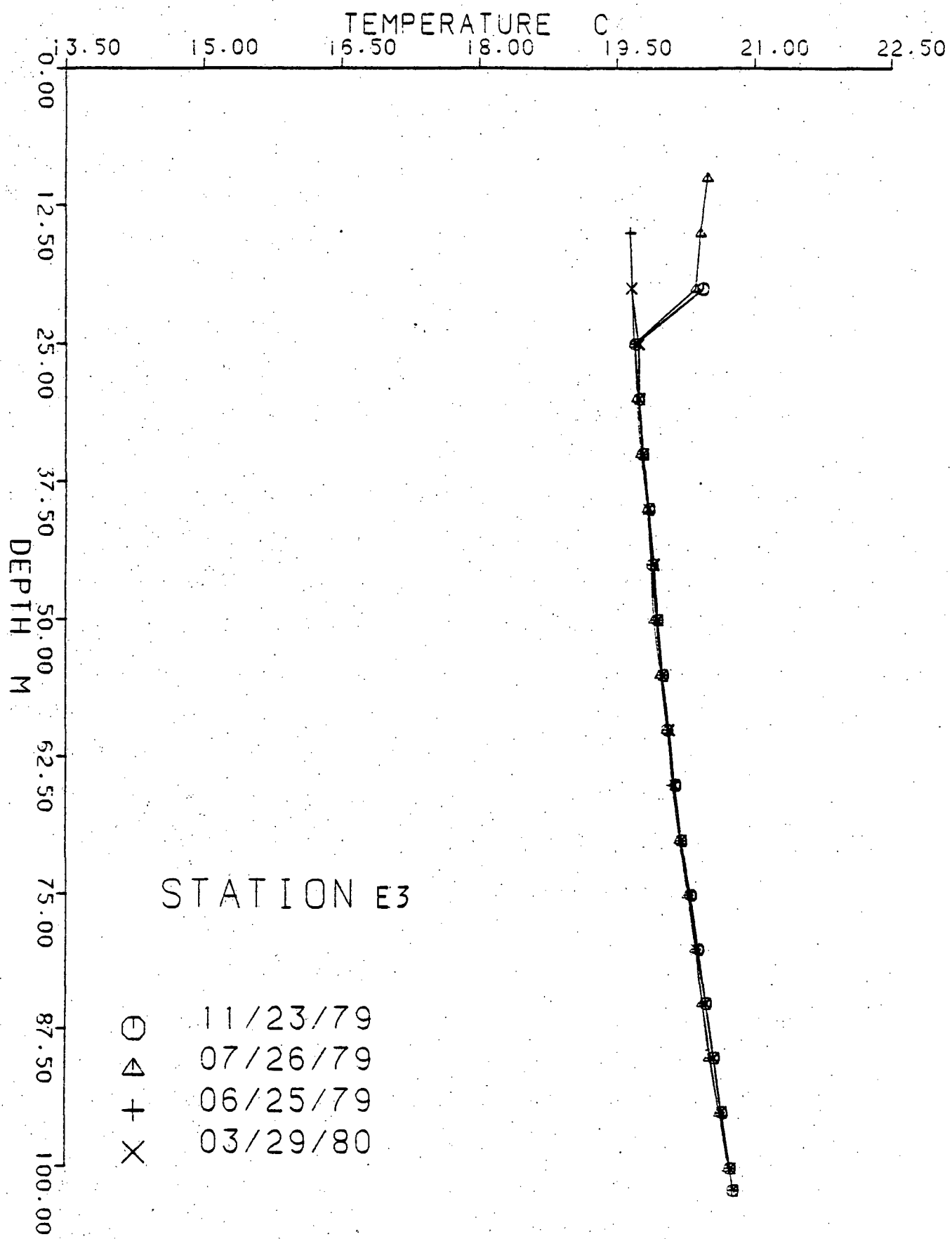
TEMPERATURE C
13.50
15.00
16.50
18.00
19.50
21.00
22.50
0.00
12.50
25.00
37.50
50.00
62.50
75.00
87.50
100.00
DEPTH M
STATION E3
11/23/79
07/26/79
06/25/79
03/29/80

Figure 7

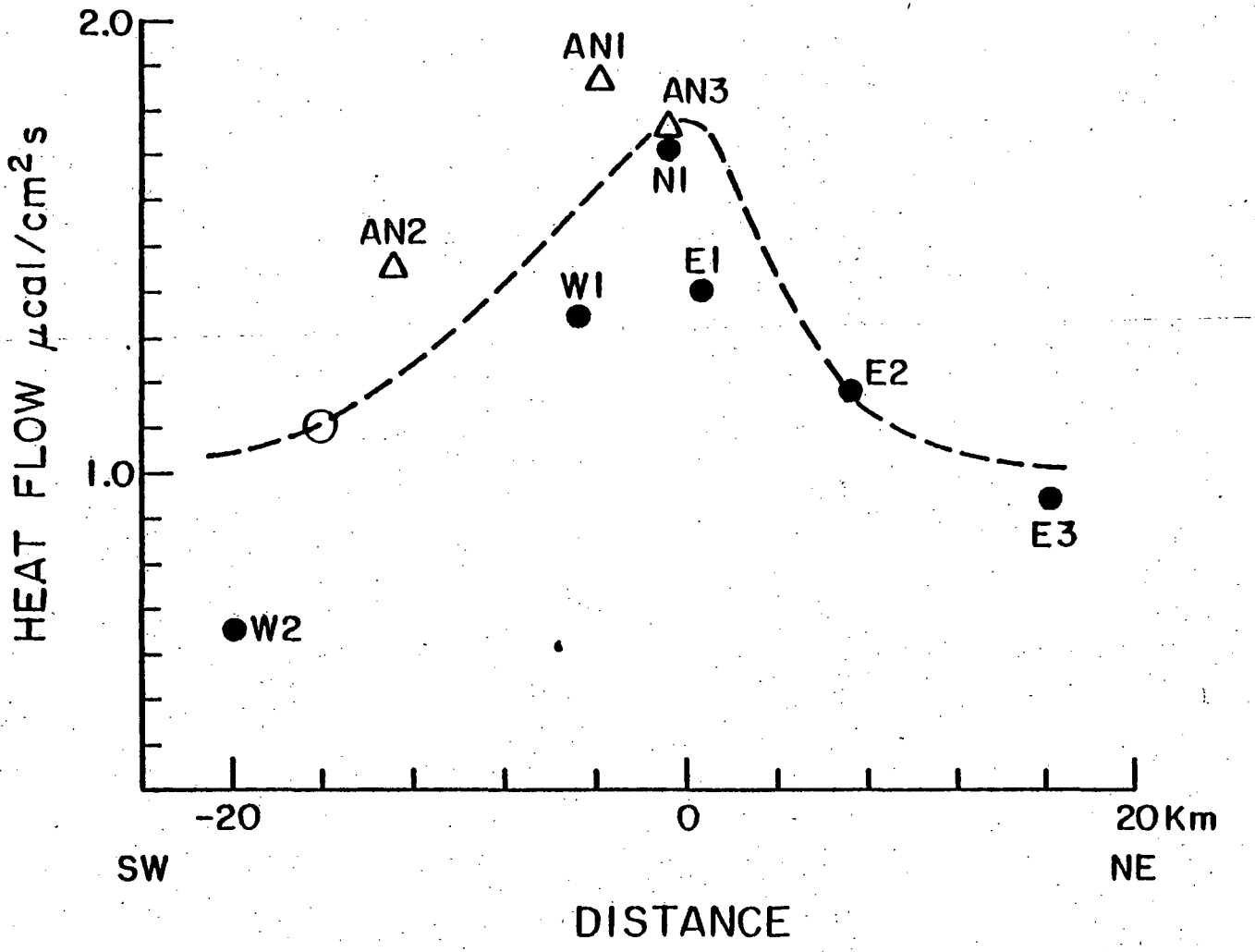
2.0
1.0
HEAT FLOW μcal/cm²s
AN1
AN3
N1
AN2
W1
E1
E2
E3
W2
-20
0
20Km
SW
NE
DISTANCE

Figure 8

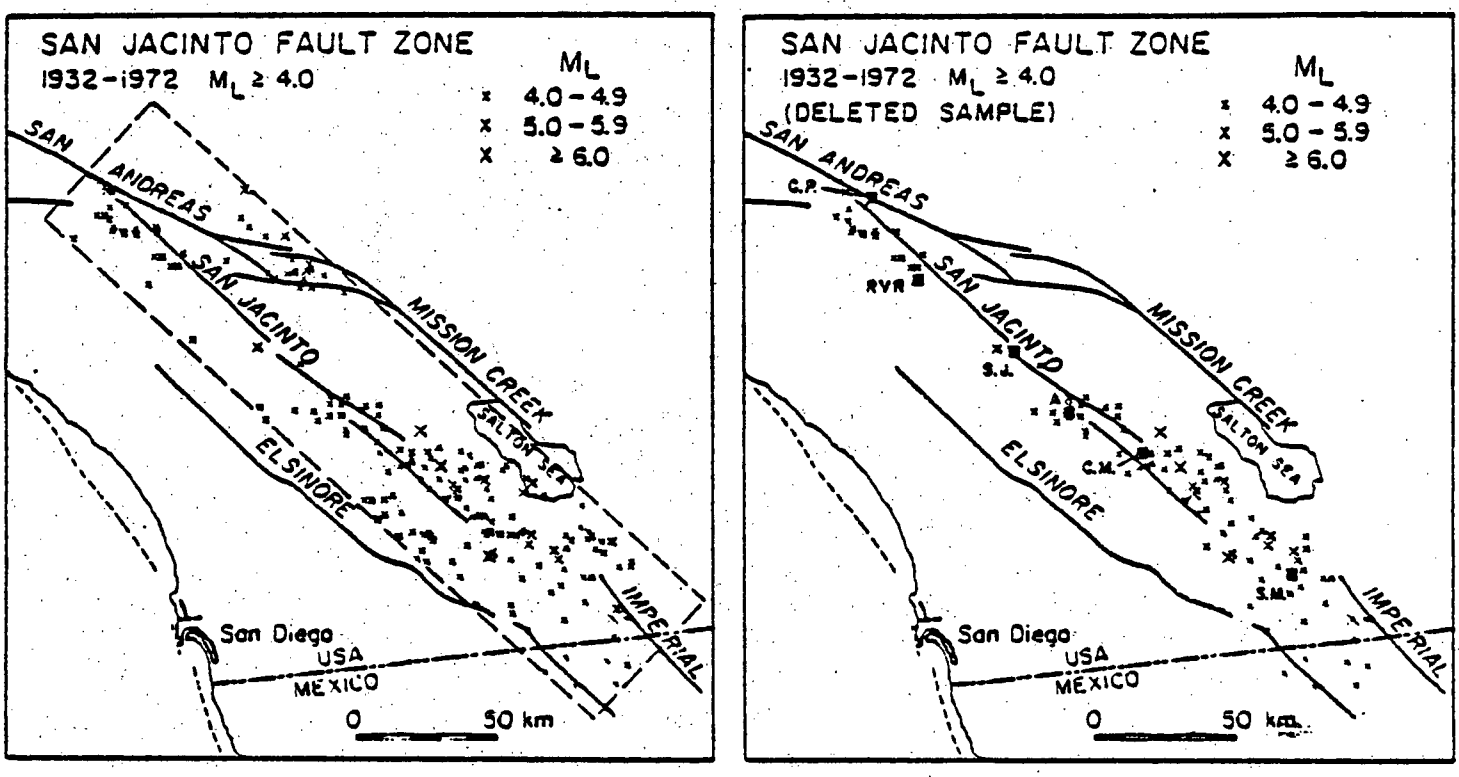
SAN JACINTO FAULT ZONE
1932-1972 $M_L \geq 4.0$
M_L
4.0 - 4.9
5.0 - 5.9
≥ 6.0
SAN ANDREAS
SAN JACINTO
MISSION CREEK
SALTON SEA
ELSINORE
IMPERIAL
San Diego
USA
MEXICO
0
50 km
SAN JACINTO FAULT ZONE
1932-1972 $M_L \geq 4.0$
(DELETED SAMPLE)
M_L
4.0 - 4.9
5.0 - 5.9
≥ 6.0
SAN ANDREAS
C.P.
RVR
SAN JACINTO
S.J.
MISSION CREEK
SALTON SEA
C.M.
ELSINORE
S.M.
IMPERIAL
San Diego
USA
MEXICO
0
50 km

Figure 9

REFERENCES

Allen, C. R., 1975, Geological criteria for evaluating seismicity: Bull. Geol. Soc. Am., 86, 1041-1057.

Birch, F., 1950, Flow of heat in the Front Range, Colorado: Bull. Geol. Soc. Am., 61, 567-630.

Brune, J. N., 1968, Siesmic moment, seismicity, and rate of slip along major fault zones: Jour. Geophys. Res., 73, 777-784.

Henyey, T. L. and G. J. Wasserburg, 1971, Heat flow near major strike-slip faults in California: Jour. Geophys. Res., 76, 7924-7946.

Lachenbruch, A. H. and J. H. Sass, 1973, Thermo-mechanical aspects of the San Andreas fault system: Stanford Univ. Publ. Ser. Geol. Sci., 13, 192-205.

Ratcliff, E. H., 1959, Thermal conductivities of fused and crystalline quartz: Brit. J. Appl. Phys., 10, 22-25.

Sass, J. H., A. H. Lachenbruch, and R. J. Munroe, 1971, Thermal conductivity of rocks from measurements on fragments and its application to heat-flow determinations: J. Geophys. Res., 76, 3391-3401.

Sharp, R. V., 1967, San Jacinto fault zone in the Peninsular Ranges of southern California: Geol. Soc. Am. Bull., 78, 705-730.

Smith, G. I., 1960, Time of last displacement on the middle part of the Garlock fault, California: U.S. Geol. Survey Prof. Paper 400-B, 280.

Thatcher, W., J. A. Hileman, and T. C. Hanks, 1975, Seismic slip distribution along the San Jacinto fault zone, southern California, and its implications: Geol. Soc. Am. Bull., 86, 1131-1139.

Whitten, C. A., 1956, Crustal movements in California and Nevada: Am. Geophys. Union Trans., 37, 393-398.